# Plasmonic effects in the neutralization of slow ions at a metallic surface

Marnik Bercx[1,4], Selma Mayda[1], Diederik Depla[3], Bart Partoens[2], and Dirk Lamoen[1]

[1]Electron Microscopy for Materials Science (EMAT) and NANOlab Center of Excellence, Department of Physics, University of Antwerp, Groenenborgerlaan 171 2020 Antwerp, Belgium.
[2]Condensed Matter Theory (CMT) and NANOlab Center of Excellence, Department of Physics, University of Antwerp, Groenenborgerlaan 171 2020 Antwerp, Belgium.
[3]Department of Solid State Sciences, Ghent University, Krijgslaan 281 (S1), 9000 Gent, Belgium.
[4]Theory and Simulation of Materials (THEOS) and National Centre for Computational Design and Discovery of Novel Materials (MARVEL), École Polytechnique Fédérale de Lausanne, Lausanne, Switzerland

2023-08-23

## Abstract

Secondary electron emission is an important process that plays a significant role in several plasma-related applications. As measuring the secondary electron yield experimentally is very challenging, quantitative modelling of this process to obtain reliable yield data is critical as input for higher-scale simulations. Here we build upon our previous work combining density functional theory calculations with a model originally developed by Hagstrum to extend its application to metallic surfaces. As plasmonic effects play a much more important role in the secondary electron emission mechanism for metals, we introduce an approach based on Poisson point processes to include both surface and bulk plasmon excitations to the process. The resulting model is able to reproduce the yield spectra of several available experimental results quite well, but requires the introduction of global fitting parameters which describe the strength of the plasmon interactions. Finally, we use an in-house developed workflow to calculate the electron yield for a list of elemental surfaces spanning the periodic table to produce an extensive data set for the community, and compare our results with more simplified approaches from the literature.

**Keywords:** Density Functional Theory, secondary electron emission, ion scattering from surfaces, plasmonic effects

# 1  Introduction

The emission of secondary electrons due to the impact of energetic primary particles is a complicated process that lies at the foundation of several surface characterization techniques. Understanding this process in the case of incident ions can also be valuable for several

applications, such as plasma display panels [1, 2] and magnetron sputtering deposition [3, 4] and the survival of freshly generated dust in post-disruption plasmas [5]. Finally, the ion-induced secondary electron yield $\gamma$ is also an important input parameter for several models related to plasma dynamics [6] or micro-plasmas [7, 8]. Despite its importance in a broad range of research fields, experimental data on the secondary electron yield is scarce, due to the difficult and specific measurement setup that is required.

Both the experimental measurement and theoretical modelling of ion-induced electron emission (IIEE) from the neutralization of incident ions has been greatly advanced by the pioneering work of Hagstrum [9–11]. His quantitative approach was built on a solid understanding of the IIEE process, but relied on an array of fitting parameters due to the lack of *ab initio* input. Cho et al. [2] used first-principles density functional theory (DFT) calculations to obtain the required density of states (DOS) and work function of various surfaces of MgO, but copied from the work of Hagstrum a set of parameters for the escape probability that were fitted to the emission spectra of He$^+$ ions on a Ge surface. We have recently published our own model, where we have made several adjustments to Hagstrum's model to remove its dependency on fitting parameters and improve the calculated yield spectra by including electron cascades in the emission process [12]. Based on first-principles DFT calculated input for the DOS and work function, our model is reasonably successful at quantitatively reproducing the IIEE yield spectra of He$^+$ and Ne$^+$ ions incident on Ge(111) and Si(111). Note that there are many other approaches discussed in the literature for the calculation of secondary electron yield. We refer the reader to the review article of Monreal [13] for an overview of the field.

In this article, we present an extension of our model to calculate the secondary electron yield of metallic surfaces based on input from first-principles DFT calculations. This involves the inclusion of plasmonic effects, which are expected to have a significant influence on the IIEE yield of metals [14–16]. After comparing the computed results with available experimental spectra, we apply the final model to a whole range of elemental surfaces spanning the periodic table.

## 2  Ion-induced Electron Emission

The secondary emission of electrons from ion bombardment is either driven by two emission mechanisms [17]: kinetic electron emission (KEE), where the excited electron energy is mainly provided by the kinetic energy of the incident ion, and potential electron emission (PEE), where the stored potential energy of the ion is the main driver of the electron excitation. For very slow incident ions, PEE is the only possible mechanism as the kinetic energy of the ion must exceed a certain threshold for KEE to occur [18, 19]. For PEE, Hagstrum considered several routes to neutralize the incoming ion [10]: Auger neutralization (AN) and resonance neutralization (RN) followed by Auger de-excitation (AD) (Fig. 1). For AN, an electron from the surface material tunnels directly into the lowest unoccupied state of the incoming ion. The energy released in this transition is passed to another electron in the material. This electron, in turn, has a probability to escape if it is excited to a state with an energy above the vacuum level $\epsilon_0$ and its momentum is properly directed with respect to the surface normal.

In the case of RN, an electron from the surface tunnels into an excited state of the incoming ion, after which the atom returns to the ground state by AD. This can occur via

1. *direct* de-excitation (dashed lines in Fig. 1c) when the electron in the excited state of the ion drops to the vacant ground state, passing the excess energy to a secondary electron inside the surface.

2. *indirect* Auger de-excitation (full lines in Fig. 1c), where an electron from inside the surface tunnels into the vacant ground state of the ion, passing the excess energy to the electron in the excited state which is subsequently ejected from the system.

The two-step process involving RN followed by AD becomes feasible only when the incident ion's excited energy levels fall within the occupied states range of the surface. As the ion gets closer to the surface, the image interaction shifts the energy levels towards the vacuum level $\epsilon_0$, possibly exceeding the Fermi level $\epsilon_F$. Therefore, the occurrence of RN depends on both the material's work function $\phi$ and the distance at which the ion gets neutralized. Due to the intricacies involved in calculating transition rates for various processes [20], we have chosen to exclude the RN/AD route from our calculations. Instead, we focus on the AN process, which is always possible for electrons with sufficient energy. For direct de-excitation, the excited secondary electron is generated inside the surface, and the situation closely resembles the AN scenario. Therefore, disregarding the RN/AD route has minimal impact on the calculated yield for this case. If the de-excitation occurs via the other path, where an electron inside the surface tunnels to the lowest occupied state and passes its energy to the resonant electron, the secondary electron will already be outside the surface and hence have a higher likelihood of contributing to the yield. Indeed, Hagstrum noted that for $Ne^+$ ions incident on molybdenum and tungsten surfaces, more ions are neutralized via the RN/AD route as the kinetic energy of the ion increases, resulting in a larger yield [21, 22]. Consequently, neglecting the RN/AD process may lead to an underestimation of the calculated yield. As a final note, in some cases it is also possible for the incoming ion to be neutralized by direct resonant neutralization to the unoccupied ground state (not shown in Fig 1). Since this is a one-electron process, it would dominate the two-electron AN process in case RN to the ground state is not energetically forbidden. However, as we focus on incident ions with high ionization energies in this work ($He^+$ and $Ne^+$), we can safely disregard this process in our model.

In our previous work [12] we presented a new model derived from Hagstrum's approach, where we include electron cascades in the secondary electron emission process, and supply the necessary input based on first-principles calculations. Including these adjustments, our calculated yield spectra matched reasonably well with the experimental results of Hagstrum for Ge(111) and Si(111). As here we want to extend our model to metallic surfaces, the rest of this section provides a brief revision of this model, recast in the context of metals. The main physical assumptions of Hagstrum's model are:

1. The surface is assumed to be smooth and without structure, i.e. no distinction is made between approach directly on an atomic site or between atoms. Moreover, an excited electron's chance of escape is only dependent on its energy and direction versus the surface normal.
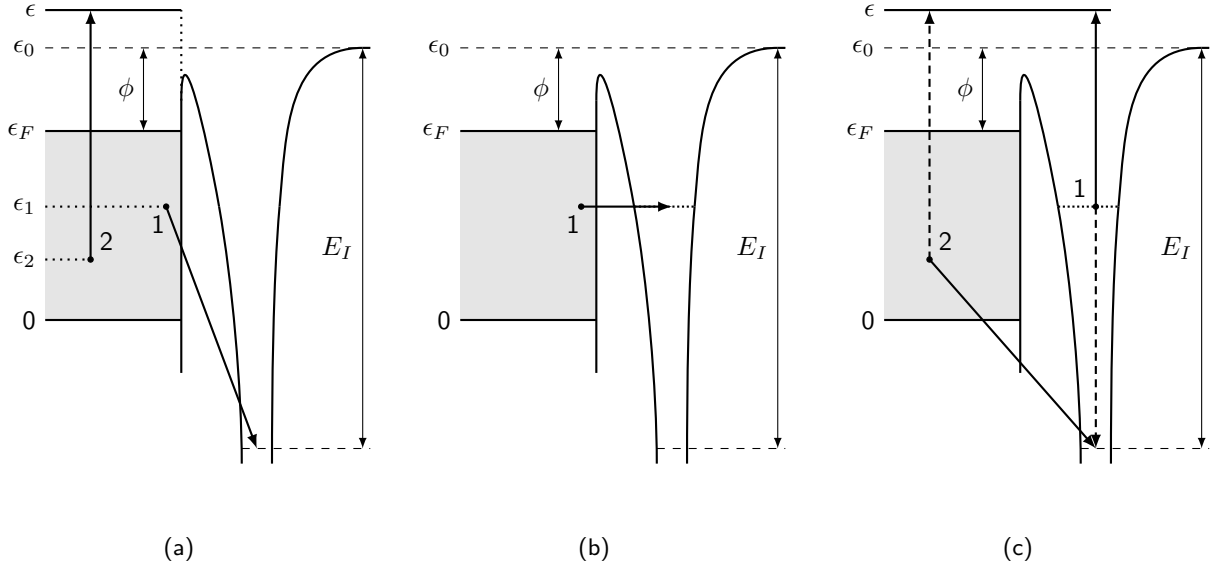
Figure 1: Schematic representations of the Auger neutralization (a), resonance neutralization (b) and Auger de-excitation (c) processes. The arrows indicate the transitions that are involved in each process. For the de-excitation, the full and dashed arrows each represent one possible way via which the de-excitation can occur. $\epsilon_1$ and $\epsilon_2$ are the initial energies of the electrons of the surface, $\epsilon$ is the energy of the excited Auger electron, $\epsilon_0$ is the vacuum level, $E_I$ the ionization energy of the incoming ion and $\epsilon_F$ is the Fermi level.

2. As the ion approaches the surface, the atomic energies are shifted due to the interaction with the induced image charge on the surface. Based on experimental observations using low-energy $He^+$, Hagstrum concluded that the shift in ionization is about 2 eV which corresponds to a neutralization distance of about 2 Å. In reality there is a probability distribution that the ions gets neutralized at a certain distance, which leads to a broadening of the energy spectra, but this is neglected.

3. No attempt is made to calculate the transition matrix elements. Instead, the probability that an electron with a certain energy participates in the AN process is simply proportional to the density of states at that energy.

We refer the reader to Hagstrum's work or our paper on semiconductors [12] for more details.

During the Auger neutralization, an electron tunnels through the surface barrier to the lowest unoccupied ionic state, transferring the excess energy to a secondary electron of the surface material (Fig. 1a):

$$\epsilon_1 + \epsilon_2 \rightarrow \epsilon + \epsilon_0 - E_I. \tag{1}$$

Here, $\epsilon_1$ and $\epsilon_2$ are the initial energies of the electrons of the surface, $\epsilon$ is the energy of the excited Auger electron, $\epsilon_0$ is the vacuum level, and $E_I$ the ionization energy of the incoming

ion. The latter is reduced by 2 eV to correct for the shift in atomic energy levels of the incoming ion due to the image interaction with the surface leading to an ionization energy of 22.58 eV and 21.56 eV for $He^+$ and $Ne^+$, respectively. The initial distribution of excited electrons is calculated using Hagstrum's approach:

$$N_i(\epsilon) = \frac{D_c(\epsilon)T\left[\dfrac{\epsilon + \epsilon_0 - E_I}{2}\right]}{\displaystyle\int_{\epsilon_F}^{\infty} D_c(\epsilon)T\left[\dfrac{\epsilon + \epsilon_0 - E_I}{2}\right]d\epsilon} \quad (\epsilon > \epsilon_F); \quad N_i(\epsilon) = 0 \quad (\epsilon \le \epsilon_F) \tag{2}$$

where $D_c$ is the density of the unoccupied states of the surface, $\epsilon_F$ the Fermi level, and $T$ is the Auger transform:

$$T\left[\frac{\epsilon + \epsilon_0 - E_I}{2}\right] = \int_0^{\epsilon_F}\int_0^{\epsilon_F} D_v(\epsilon_1)D_v(\epsilon_2) \\ \delta(\epsilon - \epsilon_1 - \epsilon_2 + \epsilon_0 - E_I)d\epsilon_1 d\epsilon_2. \tag{3}$$

Here, $D_v(\epsilon)$ is the density of the occupied states and $\delta$ is the Dirac delta function. Note that $N_i(\epsilon)$ is normalized to unity because of the assumption that every incoming ion is neutralized, producing one excited electron inside the surface. The delta function is used to assert energy conservation of the Auger neutralization process (Eq. 1).

Next, the distribution of the electrons that can escape from the surface $N_0(\epsilon)$ is calculated by multiplying $N_i(\epsilon)$ with the aptly named escape probability $P_e(\epsilon)$:

$$N_0(\epsilon) = P_e(\epsilon)N_i(\epsilon), \tag{4}$$

where the escape function is calculated based on the transmission coefficient of a step barrier (see [12]):

$$P_e(\epsilon) = \frac{1}{4\pi}\int_0^{2\pi}d\varphi\int_0^{\frac{\pi}{2}}\sin\theta d\theta \frac{4k_\perp(\theta)p_\perp(\theta)}{(k_\perp(\theta) + p_\perp(\theta))^2}. \tag{5}$$

We consider a step barrier equal to the work function $\phi$, i.e.

$$k = \sqrt{2m_e(\epsilon - \epsilon_F)/\hbar^2} \tag{6}$$

and

$$\frac{\hbar^2 k_\perp^2}{2m_e} - \phi = \frac{\hbar^2 p_\perp^2}{2m_e}. \tag{7}$$

The electron cascades are included by first considering the distribution of the electrons which did not escape the surface after neutralizing the incident ion:

$$N_c^{(2)}(\epsilon_1) = (1 - P_e(\epsilon_1))N_i(\epsilon_1). \tag{8}$$

These electrons can scatter on other electrons inside the surface, resulting in a redistribution of the electron energies:

$$\epsilon_1 + \epsilon_2 \rightarrow \epsilon + \epsilon', \tag{9}$$

where $\epsilon_1$, $\epsilon_2$ and $\epsilon$, $\epsilon'$ are the initial and final energies of the scattering electrons, respectively. The new internal distribution of excited electrons is then calculated using

$$N_i^{(2)}(\epsilon) = 2n_i \frac{D_c(\epsilon) \int_{\epsilon_c}^{\infty} d\epsilon' D_c(\epsilon') T_{ee}(\epsilon, \epsilon')}{\int_{\epsilon_c}^{\infty} d\epsilon D_c(\epsilon) \int_{\epsilon_c}^{\infty} d\epsilon' D_c(\epsilon') T_{ee}(\epsilon, \epsilon')}, \tag{10}$$

where $T_{ee}(\epsilon, \epsilon')$ is the scattering transform:

$$T_{ee}(\epsilon, \epsilon') = \int_{\epsilon_0}^{\infty} d\epsilon_1 \int_0^{\epsilon_F} d\epsilon_2 N_c^{(2)}(\epsilon_1) D_v(\epsilon_2) \delta(\epsilon + \epsilon' - \epsilon_1 - \epsilon_2) \tag{11}$$

and $n_i$ the number of excited electrons before scattering

$$n_i = \int_{\epsilon_0}^{\infty} N_c^{(2)}(\epsilon') d\epsilon'. \tag{12}$$

This process is iterated, where the total yield at step $k$ is equal to:

$$\gamma_k = \int_{\epsilon_0}^{\infty} P_e(\epsilon) \left[ N_i(\epsilon) + \sum_{s=2}^{k} N_i^{(s)}(\epsilon) \right]. \tag{13}$$

Once the difference in yield $\gamma_k$ between two cascade iterations is smaller than 0.001, the process is considered converged. We refer the reader to our previous work [12] for more details. In short, the model for the electron cascades closely follows the assumptions of Hagstrum's approach to calculate the initial distribution of excited electrons after the Auger neutralization. An electron's likelihood of participating in the scattering process is proportional to the density of occupied states $D_v(\epsilon)$. Similarly, the scattered electrons are more likely to end up with energies that correspond to a large density of unoccupied states $D_c(\epsilon)$.

# 3    Plasmonic Excitations

It is well established that plasmon excitations play an important role in the interaction of ions and metallic surfaces [14–16], so any attempt to calculate $\gamma$ for a broad range of metals has to include a suitable implementation of these collective electron excitations. This also becomes clear when comparing the results based on the model described in the previous section for $He^+$ and $Ne^+$ incident on Mg(100) with the experimental result of Baragiola and Dukes [14] in Fig. 2. The experimental yield spectrum is severely overestimated, especially at higher energies. Both experimental spectra also present a rather distinct feature: above $\epsilon_k \approx 7 - 8$ eV there is a plateau in the yield spectrum for both $He^+$ and $Ne^+$, which is not reproduced by the model described in the previous section.
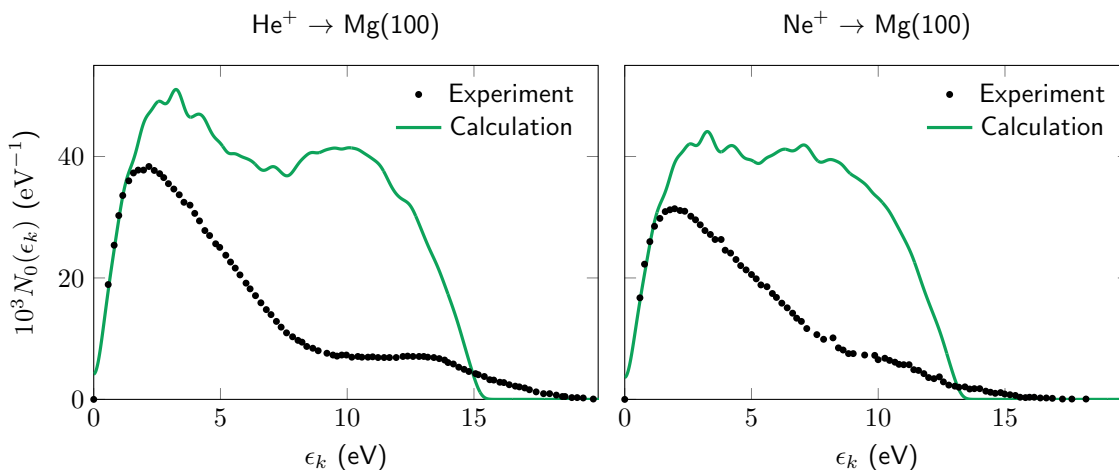


Figure 2: Comparison of the experimental secondary electron yield distribution with the calculated ones for $He^+$ (left) and $Ne^+$ (right) incident on Mg(100), without the inclusion of plasmonic effects.

We consider two mechanisms to induce plasmonic excitations in our model. The first, surface resonance excitation, is introduced as a competing process for the Auger neutralization. The model for semiconductors considers the excess energy of the neutralization of every incoming ion to always result in the excitation of a single electron. There are, however, other processes that are in direct competition with the Auger mechanism. First, the released energy can produce a photon which is subsequently emitted from the material. However, this radiative process is mostly considered negligible for low ion energies [23], and only contributes significantly for highly charged ions at grazing incidence. More important are collective charge density oscillations, i.e. plasmon excitations, first considered as a potential competing excitation mechanism by Apell [24]. Other theoretical work also confirms the importance of plasmon mechanisms for the ion neutralization process [23, 25, 26].

However, considering the electronic structure of the (100) surface of Mg in Fig. 3a, a resonant excitation mechanism alone is not sufficient to explain the experimental electron energy

distribution of He$^+$ on Mg in Fig. 2. The highest energy electrons in the excited spectrum are produced by electrons near the Fermi energy. The plasmon energy of Mg is approximately 10.6 eV [27], and the work function $\phi = 3.66$ eV [28]. For a singly charged He$^+$ ion, the image-corrected ionization energy is $E_I = 22.58$ eV. If the electrons close to the Fermi level in Mg are the ones to neutralize the incoming ion, an energy of up to 18.94 eV is released. Since the width of the density of occupied states is $\Delta \epsilon_v = 6.96$ eV, the lowest energy released by the ion neutralization is $E_I - \Delta \epsilon_v - \phi = 11.98$ eV. If the plasmon activity is only described by a resonant process, we expect very few plasmon excitations, even if the plasmon resonance peak is significantly broadened by the short plasmon lifetime. There is, however, a second plasmon excitation mechanism which is not resonant in its nature. As the excited electrons travel through the material, they leave behind a wake of electron density fluctuations, leading to the possibility of energy loss through volume plasmon excitations (Fig. 3b) in case the electrons have sufficient energy [29]. This excitation process does not have a resonance condition, i.e. as long as the excess electron energy is above the plasmon energy, the electron can excite a plasmon, losing energy in the process [15].
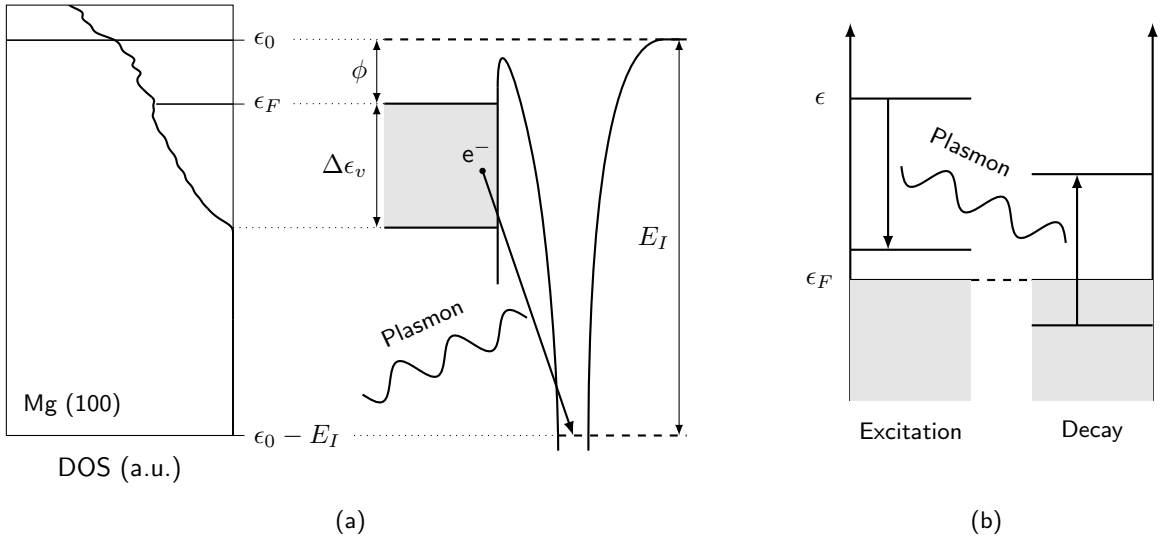


Figure 3: Energy diagrams of resonant surface (a) and volume plasmon (b) excitations. (a) also shows the DOS of Mg (110), with the energies aligned to the diagram.

In order to include the plasmonic excitations in our model, we describe them as Poisson point processes [30], i.e. the intervals $T_p$ between events follow an exponential distribution [31]:

$$f_{T_p}(t) = \lambda_p e^{-\lambda_p t}, \tag{14}$$

for a process $p$, i.e. volume plasmon excitation ($vp$), surface plasmon excitation ($sp$) or Auger neutralization ($aug$). The excitation rate of volume plasmons with energy $E_{vp}$ can be related

to the dielectric function $\varepsilon(\omega)$ through the volume loss function $L$ [32]:

$$\lambda_{vp}(E_{vp}) \quad \sim \quad L(E_{vp}) = \text{Im}\left[-\frac{1}{\varepsilon(E_{vp})}\right] \tag{15}$$

$$\lambda_{vp}(E_{vp}) \quad = \quad c_{vp} \cdot \text{Im}\left[-\frac{1}{\varepsilon(E_{vp})}\right], \tag{16}$$

where $c_{vp}$ is a proportionality constant and Im represents the imaginary part. Each of the possible energy losses $E_{vp}$ are considered as competing Poisson point processes. However, as the excited electron cannot wind up in an occupied state, it cannot lose more energy than its energy relative to the Fermi level $\epsilon - \epsilon_F$. Writing the average travel interval of the excited electrons as $t_e$, the probability for an electron at energy $\epsilon$ of exciting a plasmon with energy $E_{vp} < \epsilon - \epsilon_F$ is (see Section 1 in the Supplementary material):

$$P_{vp}(\epsilon, E_{vp})dE_{vp} \quad = \quad \frac{c_{vp}L(E_{vp})dE_{vp}}{\int_0^{\epsilon-\epsilon_F} c_{vp}L(E)dE}\left[1 - e^{-\left(\int_0^{\epsilon-\epsilon_F} c_{vp}L(E)dE\right)t_e}\right] \tag{17}$$

$$= \quad \frac{L(E_{vp})dE_{vp}}{\int_0^{\epsilon-\epsilon_F} L(E)dE}\left[1 - e^{-\left(\int_0^{\epsilon-\epsilon_F} L(E)dE\right)c_{vp}t_e}\right] \tag{18}$$

The product $\kappa_v = c_{vp} \cdot t_e$, the combination of the prefactor of the rate $\lambda_{vp}$ and the average travel interval of the excited electrons, is a measure of the likelihood of plasmon excitations during the PEE process. We treat it as a parameter of the model.

For the surface plasmons, a plasmon excitation can occur instead of a single-electron excitation when the energy released in the neutralization of the incoming ion is close to that of the surface plasmon. To determine the possibility of a surface plasmon excitation, both processes are once again modeled as Poisson point processes, i.e. by considering the exponential distributions

$$f_{T_{sp}}(E_{sp}, t) = \lambda_{sp}(E_{sp})e^{-\lambda_{sp}(E_{sp})t} \tag{19}$$

$$f_{T_{aug}}(t) = \lambda_{aug}e^{-\lambda_{aug}t}. \tag{20}$$

The probability that the plasmon excitation occurs before the Auger neutralization is then

$$P_{sp}(E_{sp}) = \text{Pr}\{T_{sp} < T_{aug}\} = \frac{\lambda_{sp}(E_{sp})}{\lambda_{sp}(E_{sp}) + \lambda_{aug}} \tag{21}$$

Where Pr is used to indicate the probability of a surface plasmon excitation occuring before the Auger neutralization. The surface plasmon excitation rate is calculated from the dielectric response of the surface using the surface energy loss function [32]:

$$\lambda_{sp}(E_{sp}) = c_{sp} \cdot \text{Im}\left[-\frac{1}{\varepsilon(E_{sp}) + 1}\right], \tag{22}$$

9

where $c_{sp}$ is once again a proportionality constant. The expression for the probability of a plasmon excitation when an energy $E_{sp}$ is transferred to the incoming ion becomes:

$$P_{sp}(E_{sp}) = \frac{c_{sp} \cdot \text{Im}\left[-\frac{1}{\varepsilon(E_{sp})+1}\right]}{c_{sp} \cdot \text{Im}\left[-\frac{1}{\varepsilon(E_{sp})+1}\right] + \lambda_{aug}} = \frac{\frac{c_{sp}}{\lambda_{aug}}\text{Im}\left[-\frac{1}{\varepsilon(E_{sp})+1}\right]}{\frac{c_{sp}}{\lambda_{aug}}\text{Im}\left[-\frac{1}{\varepsilon(E_{sp})+1}\right] + 1} \tag{23}$$

where the ratio $\kappa_s = c_{sp}/\lambda_{aug}$ is treated as a second parameter of the plasmon model[1]. In this description, it is assumed that the Auger neutralization rates are similar for the various ion material combinations and independent of the energy transferred to the secondary electron.

A more detailed derivation of Eqs. (17) and (23) can be found in Section 1 of the Supplementary material, along with a description of the exact implementation of the plasmonic excitations in the model. In short, the surface plasmon excitation probability (Eq. (23)) is used to remove a fraction of the energy distribution passed to the valence electrons in the Auger neutralization. The implementation of the volume plasmon is more complicated, as an electron traveling to the surface can excite volume plasmons with a range of energies $E_{vp}$. Moreover, volume plasmons decay into single particle excitations [33], and hence the spectrum of excited plasmons has to be considered for calculating a new distribution of excited electrons resulting from plasmon decay.
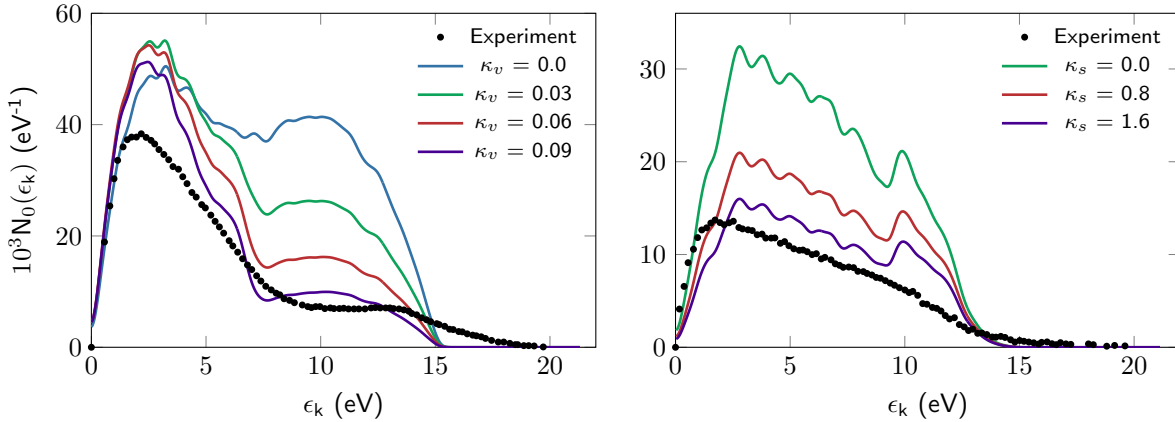


Figure 4: Influence of the volume ($\kappa_v$) and surface ($\kappa_s$) plasmon parameter on the PEE spectra of He$^+$ incident on Mg (100)(left figure) and Be (001) (right figure) surfaces. The experimental data are taken from [15].

Figure 4 shows the influence of increasing the volume and surface plasmon parameters on the spectra of He$^+$ incident on Mg(100) and Be(001) surfaces, respectively. As previously discussed, surface plasmons are unlikely to be excited during the neutralization of He$^+$ on

---

[1]We take this ratio to be the parameter - instead of its inverse - so that the amount of plasmonic activity is directly proportional to the parameter, which is more intuitive. This also allows us to turn off surface plasmons by setting the parameter to zero.

Mg, so this allows us to isolate the influence of volume plasmons. Similarly, the large plasmon frequency of Be (See Fig. 5) means that surface plasmons, having a lower frequency than volume plasmons, play a much larger role in the spectrum of Be. For Mg, volume plasmon excitations result in a large reduction of the yield spectrum at higher energies. By increasing the participation of volume plasmons through the parameter $\kappa_v$, we are able to match the experimental spectrum much more closely, largely reproducing the "plateau" feature a higher energies which was missing from our previous results (cf. Fig. 2). For the Be spectrum, increasing surface plasmon resonances through $\kappa_s$ results in an overall reduction of the yield spectrum, most likely due to the broad plasmon peak in the surface energy loss function of Be (Fig. 5).
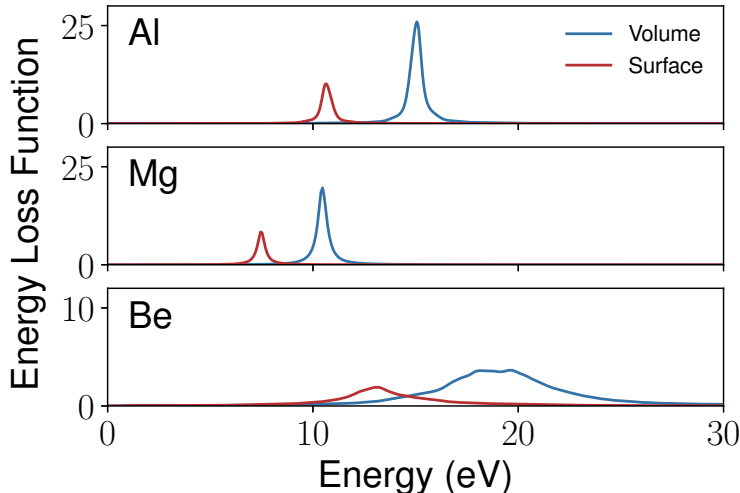


Figure 5: Volume and surface energy loss functions of Al, Mg an Be, calculated from the dielectric function of the bulk system of each element.

Although it would be possible to fit the plasmon parameters $\kappa_v$ and $\kappa_s$ for each ion/surface combination, similar to how Hagstrum fitted the escape function parameters $\alpha$ and $\beta$, this would remove any predictive capability of the model. Hence, we have fitted a *single* set of parameters to the available quantitative experimental data[2] for He$^+$ and Ne$^+$ ions incident on Al and Mg from Baragiola et al. [15], as well as Takeishi and Hagstrum's results for Ni(111) [34] and Cu(110) [35]. Unfortunately, as Baragiola et al. did not specify the surface orientation of each metal, we compare the experimental result to an average of our calculated results. Based on an interactive Jupyter notebook, we first explored the influence of the parameters on the calculated parameters for each surface to ascertain a reasonable range for the fitting procedure. Next, we take the difference of the experimental and calculated values for each experimental data point and sum over their absolute values for each spectrum, normalizing each to the number of experimental data points to give each spectrum the same weight. Based on this analysis, the optimal values for the plasmon parameters are $\kappa_v = 0.11$ and $\kappa_s = 1.6$.

---

[2]Note that there are more experimental spectra available. Their exclusion is discussed in the next section.

# 4    Computational Details

Hagstrum's model requires the density of states of the occupied and unoccupied ($D_v(\epsilon)$ and $D_c(\epsilon)$) states as input, as well as the vacuum level. The density of states and the vacuum level of all metal surfaces are calculated using a DFT approach, as implemented in the Vienna Ab initio Simulation Package [36–38] (VASP). Within the projector augmented wave [39, 40] (PAW) formalism, the recommended number of valence electrons is included for all metals. The energy cutoff is set at 500 eV in order to obtain a well converged plane wave basis set, and the exchange correlation energy is calculated using the generalized gradient approximation (GGA) of Perdew-Burke-Ernzerhof [41] (PBE). For sampling the Brillouin zone, Monkhorst-Pack [42] k-point mesh is used for which the spacing in each direction is smaller than 0.05 $\text{Å}^{-1}$.

To simulate a surface within the periodic boundary framework of VASP, it is conventional to take a slab approach, where a certain number of atomic layers are separated by a suitably large vacuum layer. We take the structures of all surfaces from the supplementary material of De Waele et al. [43] and subsequently optimize the geometry using the computational parameters described in the previous paragraph. The vacuum level is obtained by averaging the one-electron electrostatic potential over planes parallel to the surface and determining the potential in the vacuum, which should be constant in case the vacuum layer is sufficiently thick. The work function $\phi$ of the surface is then calculated by comparing the vacuum level with the top of the Fermi level $\phi = \epsilon_0 - \epsilon_F$.

The optical properties of the bulk are calculated within the Random Phase Approximation (RPA), using the long wavelength expression for the imaginary part of the dielectric function. The real part of the dielectric tensor is determined using the Kramers-Kronig relations. For the damping parameter in the Drude expression of the intraband part of the dielectric tensor a value of 50 meV is used.

# 5    Comparison with experiment

Based on the analysis in Section 3, the optimal values for the plasmon parameters are $\kappa_v = 0.11$ and $\kappa_s = 1.6$. Now that the model plasmon parameters $\kappa_v$ and $\kappa_s$ are fixed, we first compare the calculated secondary electron emission spectra for the surfaces of the metals for which experimental spectra are available. The results for the work function and calculated yields are compared with the experimental values [15, 35, 43] in Table 1. The calculated work functions are fairly close to the experimental ones for most surfaces. For Be, there is a significant difference in the calculated work function of the various surfaces. As was noted in the recent work of Tolias [44], there has been some debate on the work function of Be, for which both values around 4 eV and 5 eV have been reported in the literature. Nowadays, the general recommended value for the work function of Be is 4.98 eV, as reported in the reference work of Michaelson [45]. Earlier values below 4 eV are believed to be due to the presence of oxygen contamination of the surface, which was confirmed Green and Bauer [46].

They specifically studied the (001) surface of Be, obtaining a work function of at least 5.10 eV for the cleanest surface studied, which corresponds fairly well with our calculated value in Table 1.

There is also a good agreement between the calculated and experimental yield of $He^+$ and $Ne^+$ ions on Al, Mg and Ni, both for the total yield as well as the yield spectra (Fig. 6). For Al, our model tends to underestimate the total secondary electron emission. Comparing the full emission spectra, there is a feature of the experimental spectra that is missing in our computational results: the high energy tail of the spectrum. Hagstrum [11] already investigated the influence of the kinetic energy on the spectrum of $He^+$ on Ge(111), and found that increasing the kinetic energy of the ion leads to a broader tail of the spectrum at high energies. A similar result was found for $Ne^+$ on Al by Baragiola et al. [14], who also demonstrated an overall gain in electron yield when the kinetic energy is increased. Hagstrum introduced a broadening in the Auger transform to simulate the kinetic effects, however, as the difference is rather minor, we simply stick to a general 0.2 eV Gaussian broadening of the yield spectra for visual purposes.

In contrast with the results for Al and Mg, there is a much larger difference in the yield results for the different surfaces of Be, which can be expected considering the larger variation in the surface work function. Baragiola et al. [15] did not specify the Be surface for their PEE results, which complicates the quantitative comparison of our computational results with experiment, and hence we did not include them in our fitting procedure for the plasmon parameters. It is reassuring to see that a single set of plasmon parameters is able to reproduce a lot of varied experimental data adequately, which to some extent validates our approach in treating them as model parameters.

Table 1: Calculated work functions $\phi$ and PEE yields $\gamma$ for each of the surfaces, compared with the available experimental data. For the work function of Mg and Be we do not have specific data for each surface. Similarly, we only know the surface for the yield results of Cu and Ni.

| Element | Surface | $\phi$ (eV) | $\phi_{exp}$ (eV) | $\gamma^{He}$ | $\gamma^{He}_{exp}$ | $\gamma^{Ne}$ | $\gamma^{Ne}_{exp}$ |
|---------|---------|-------------|-------------------|---------------|---------------------|---------------|---------------------|
| Al | (111) | 4.05 | 4.28 | 0.193 | 0.231 | 0.157 | 0.202 |
|    | (100) | 4.26 | 4.36 | 0.175 | " | 0.141 | " |
|    | (110) | 4.04 | 4.21 | 0.195 | " | 0.159 | " |
| Mg | (100) | 3.65 | 3.66 | 0.286 | 0.257 | 0.222 | 0.202 |
|    | (001) | 3.7 | " | 0.242 | " | 0.195 | " |
|    | (110) | 3.49 | " | 0.316 | " | 0.245 | " |
| Ni | (111) | 5.05 | 5.28 | 0.173 | 0.175 | 0.142 | 0.124 |
|    | (100) | 4.91 | 5.23 | 0.181 | - | 0.15 | - |
|    | (110) | 4.67 | 4.64 | 0.203 | - | 0.171 | - |
| Cu | (110) | 4.4 | 4.48 | 0.145 | 0.155 | 0.12 | 0.12 |
|    | (111) | 4.77 | 4.91 | 0.125 | - | 0.101 | - |
|    | (100) | 4.52 | 4.57 | 0.139 | - | 0.114 | - |
| Be | (100) | 4.5 | 4.98 | 0.083 | 0.117 | 0.054 | 0.095 |
|    | (001) | 5.31 | " | 0.049 | " | 0.029 | " |
|    | (110) | 3.82 | " | 0.119 | " | 0.081 | " |
| W | (111) | 4.15 | 4.38 | 0.161 | 0.292 | 0.124 | 0.224 |
|   | (100) | 4.1 | 4.57 | 0.158 | " | 0.121 | " |
|   | (110) | 4.79 | 5.31 | 0.117 | " | 0.082 | " |
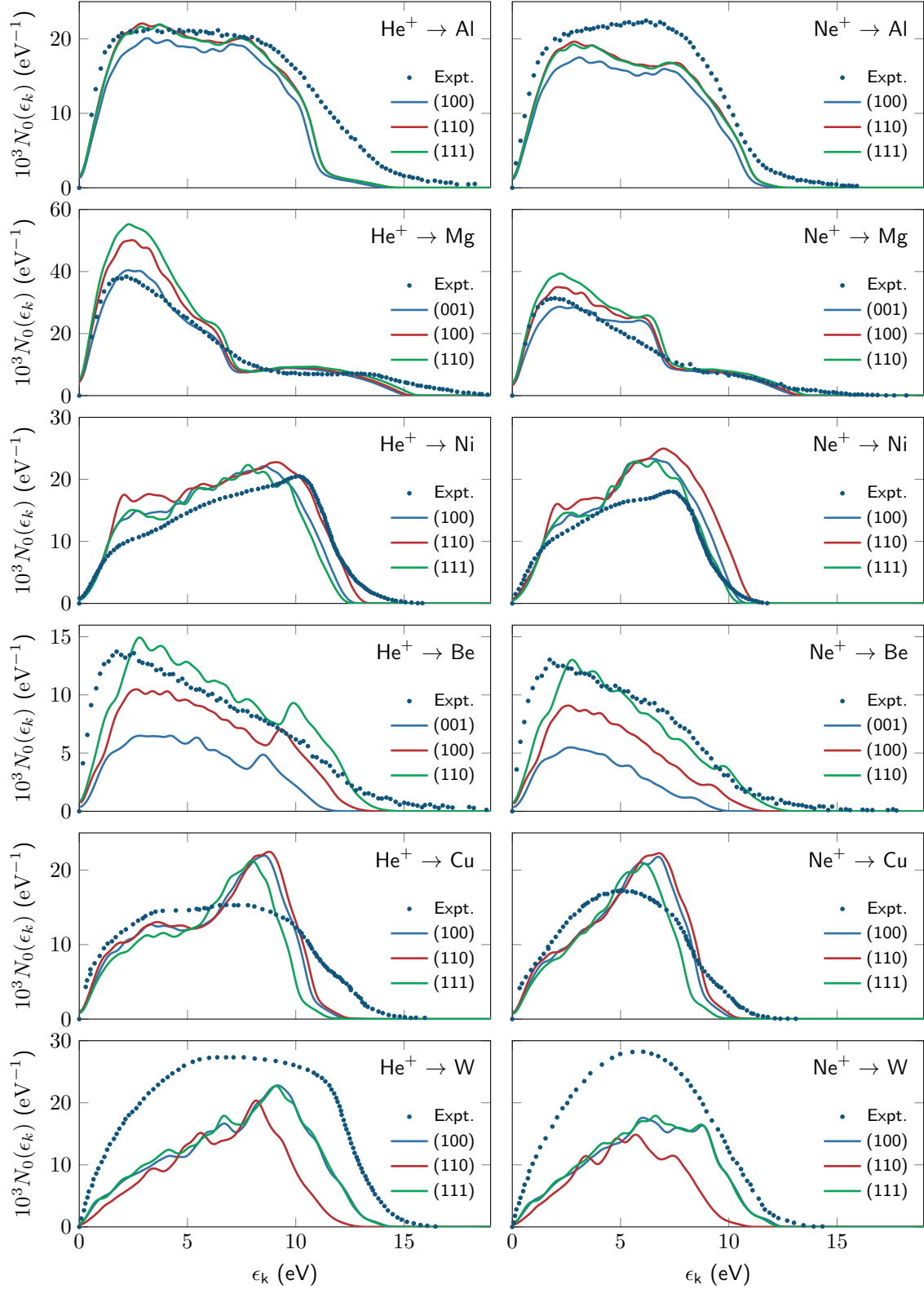
Figure 6: Experimental and calculated yield spectra for incoming He$^+$ and Ne$^+$ ions on the chosen surfaces of Al, Mg and Ni. The optimal values for the plasmon parameters are $\kappa_v = 0.11$ and $\kappa_s = 1.6$.

For Cu(110), the total yield is quite close to the experimental value, but the calculated spectrum shape differs quite significantly from the experimental one, independently of the choice of plasmon parameters. As discussed by Goebl et al. [47], the Auger neutralization rate $\lambda_{aug}$ can depend significantly on the electronic state ($s$, $p$, $d$). In fact, Goebl et al. had specifically investigated the influence of the electron orbital on the neutralization rate for noble metals (Cu, Ag and Au), and found that the rate due to $d$ electrons can be an order of magnitude higher compared to $s$ or $p$. To analyze whether this has a large effect on the yield, we implemented an input argument in the yield calculation that allows the user to give more weight to the $d$ orbitals in the neutralization of the incoming ion. However, as we can see in Fig. 7, even when we increase the weight of the $d$-orbitals by an order of magnitude, the influence on the final yield spectrum is negligible. Looking at the orbital projected density of states, this is not surprising, as the electronic states close to the Fermi level already largely correspond to $d$ orbitals. Currently, it is unclear as to why there is such a discrepancy between the calculated and experimental yield distributions of Cu(110).
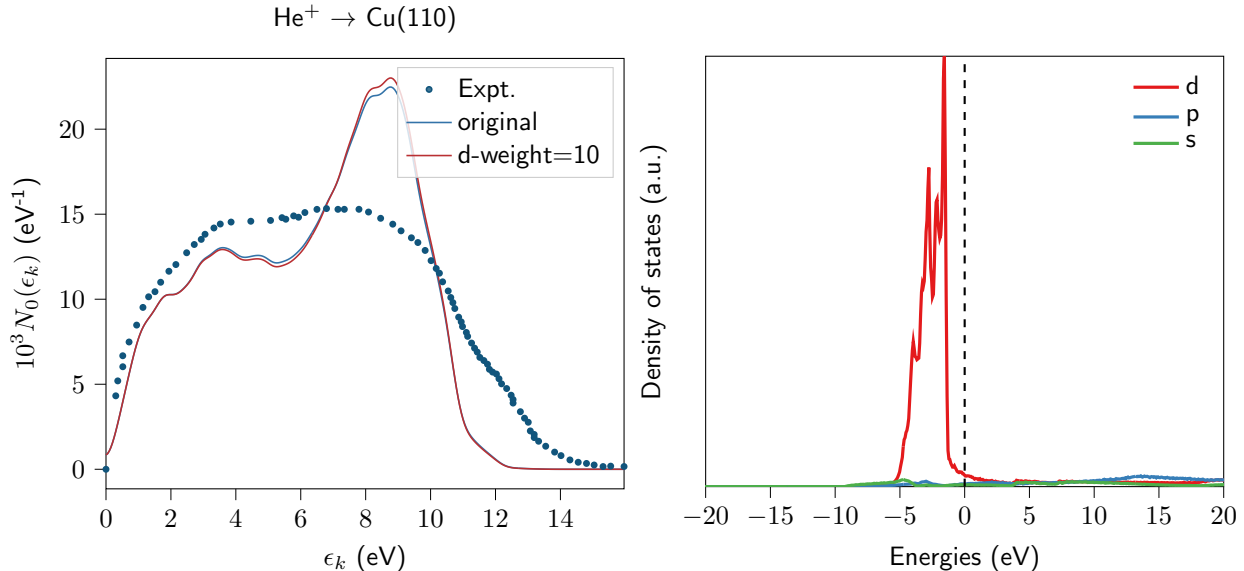


Figure 7: Influence of increasing the likelihood of $d$-electrons neutralizing the incoming ion.

Note that for W, the calculated spectrum is consistently lower than the experimental one from Hagstrum. At first glance, this seems to be related to the work function, as the position of the high energy tail is lower for the computational result. However, according to the results in Table 1, the computational work functions are lower for each surface compared to experiment. Because of this discrepancy, we did not consider W when fitting the plasmon parameters.

So far the discussion has been limited to $He^+$ and $Ne^+$ ions. For $Ar^+$, the calculated yield spectra are significantly lower than the experimental ones for most metals. This can be related to the fact that we do not consider resonance neutralization (See Fig. 1) in our calculations.

Although Auger neutralization is expected to be the dominant process, neglecting RN can have a larger effect for ions with a lower ionization energy. To understand this, consider what happens when an electron first neutralizes the incoming ion via a resonant tunneling process, and subsequently is excited to an energy above the vacuum level via Auger de-excitation. Compared to an electron that is excited inside the surface via AN, this electron is excited in the (approximately) spherical potential well of the ion. If the energy of the electron is higher than the vacuum level, the escape probability of this electron is much higher than that of an electron excited inside the surface. This difference in escape probabilities is especially large when the excited energy level is only slightly above the vacuum level, as in this case the excited electron in the surface can only escape in case its wave vector is directed almost straight at the surface.

For ions with a low ionization energy, a much larger fraction of the electrons are excited to an energy close to the vacuum level. If the electrons are excited via AN, their escape probability is low, especially when compared to RN+AD. Hence, even though only a small fraction of ions are neutralized via the latter process, the resulting electrons can make up a significant portion of the final electron yield. Although we could introduce the RN+AD process via another fitting parameter, it would be better to try and determine the likelihood of either process by calculating their rates for a model system as done by Goebl et al. [47]. This is, however, beyond the scope of the present work.

# 6  High-throughput results

Although it is gratifying to see that our model is able to reproduce both the experimental PEE yield values and spectra of many elemental surfaces, the purpose of the model is to predict the yield of surfaces for which no experimental results are available. This section presents a high throughput screening of a list of elemental surfaces spanning the periodic table, based on the workflow discussed in Sec. 4 of the Supplementary material. As is described there, the calculation of the surface properties for our model input requires a choice of sufficient atomic layers and vacuum thickness. Fortunately, here we can rely on the extensive testing of De Waele et al. [43], instead of performing the necessary convergence tests ourselves. Based on the details provided in the supplemental material of their paper, we have calculated the required input[3] for our version of Hagstrum's model for all of the tabulated surfaces. Using the model plasmon parameters from our fitting procedure, we have then calculated the total yield for $He^+$ and $Ne^+$ for each surface. Figures 8 and 9 show a map of the averaged total yield for $He^+$ and $Ne^+$ on the periodic table.

The average yield of the group IA elements is excessively high. This is a result of the combination of the low work functions of the surfaces of these elements as well as their small width of the density of occupied states $D_v(\epsilon)$. The latter increases the yield because the average energy of an electron is higher in case the electrons are all close to the Fermi level. Hence, due to these two properties, the electrons only have to overcome a relatively small barrier when trying to escape, and there are always relatively high energy electrons that

---

[3]Note that this input cannot simply be extracted from the output files of De Waele et al., as our model needs the density of states for a large number of unoccupied bands.

17

participate in both the Auger neutralization and the electron scattering processes. Most likely, our model is rather optimistic in its treatment of the electron scattering, as it does not consider the depth of the scattering electrons, allowing them a chance to escape at every iteration. This results in an overestimation of the yield for these elements, as well as other elements with similar surface properties (Ca, Y, Sc).
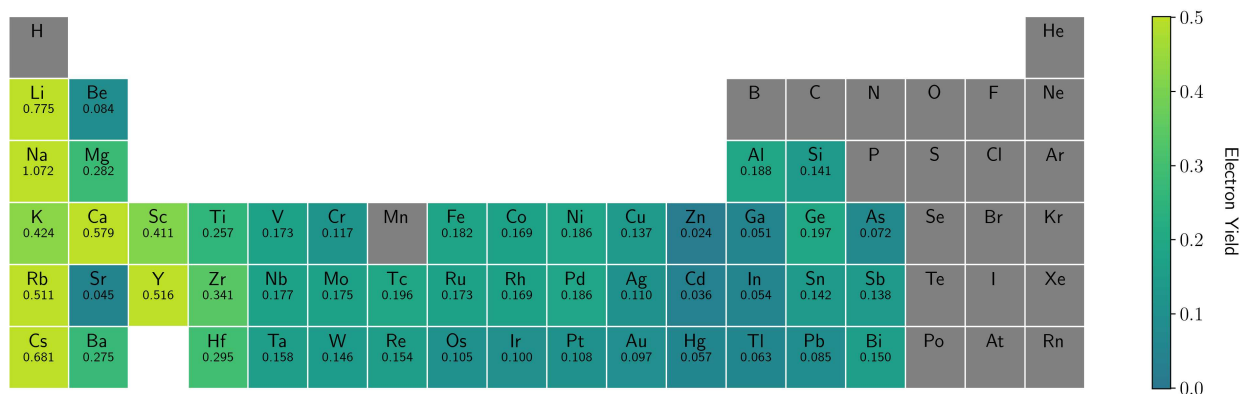


Figure 8: Average yield results for He$^+$ ions on the surfaces of the studied elements. The elements in gray were not considered in the calculations.
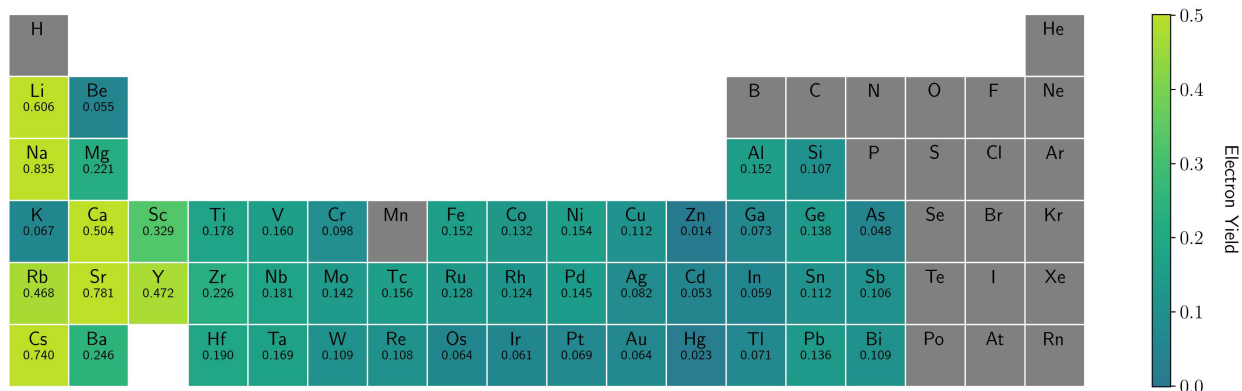


Figure 9: Average yield results for Ne$^+$ ions on the surfaces of the studied elements. The elements in gray were not considered in the calculations.

On the other side of the periodic table, elements with full $d$ orbitals and only a couple of electrons in the $s$ and/or $p$ orbitals (group 11-13, excluding Al) have a noticeably lower yield. This is connected to the electronic structure of these elements near the Fermi level. Figure 10 compares the projected DOS of Ni (100) with two group 11-13 elements: Cu (100) and Zn (100). For all of these surfaces, most of the occupied states near the Fermi level correspond to $d$ states. However, for Zn (100) these lie significantly below the Fermi level, which means that the average energy of electrons that participate in the Auger neutralization

and electron scattering processes is relatively low. This reduces the average energy of the excited electron, which results in a lower chance of escape and hence a lower yield. The electronic structures of other elements with full $d$ orbitals is similar, resulting in a lower yield for groups 11-13. Cu, and by extension Ag and Au, suffer from a similar effect, but to a lesser extent because the $d$ states are closer to the Fermi level. Finally, this also explains the relatively low results for $He^+$ ions on K, Sr and Ba.
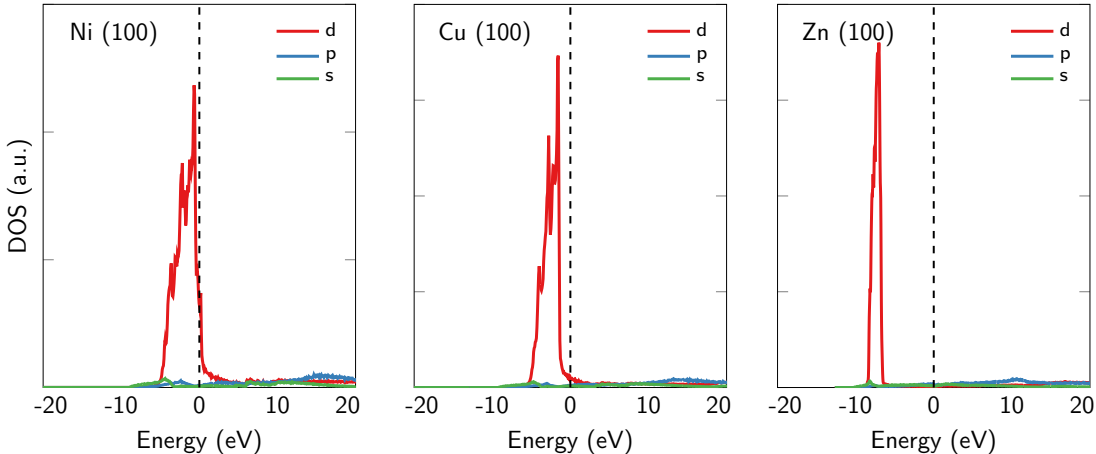


Figure 10: Projected density of states of Ni (100), Cu (100) and Zn (100).

The yield for $Ne^+$ results in a reduction for the yield for most elements compared to $He^+$, which is to be expected considering the lower ionization energy of $Ne^+$. There are some notable exceptions, however, such as Sr, Sn, Pb and Cs. Hagstrum also found lower yield values for $He^+$ compared to $Ne^+$ for ions with higher kinetic energies on Mo and W surfaces. His explanation of the increased $Ne^+$ is the increased resonance neutralization (RN) of the incoming $Ne^+$ ion, followed by Auger de-excitation (AD). As discussed in Section 2, electrons emitted from the surface via the RN/AD route have a higher likelihood of escaping the material as well as a higher maximum of their kinetic energy, increasing the total electron yield. However, we exclusively consider direct Auger neutralization and neglect the kinetic energy of the incident ion in our model, and hence this observation cannot explain the increased yield of $Ne^+$ in our results.

Instead, the increased yield for $Ne^+$ for Sr, Sn and Pb can be explained by the fact that due to the lower ionization energy of $Ne^+$, the deep $d$ orbitals can no longer neutralize the incoming ion, which means that only the higher energy $s$ and $p$ electrons take part, resulting in a higher average energy of the excited Auger electrons. For $He^+$ on Cs, there is an increased resonance between the energy released during the neutralization and the surface plasmon excitation. Interesting here is also the low average yield value for $Ne^+$ on K. This is due to the fact that the $3p$ orbitals of K are just barely able to neutralize the incoming ion, resulting in a large fraction of electrons in the excited density that are just above the vacuum level, and hence a severely reduced yield.

It is conceivable that these lower shell electrons have very little overlap between their wave function and that of the lowest occupied state of the incoming ion, resulting in a low likelihood of them neutralizing the ion. In this case, the participation of the higher energy $s$ and $p$ states increases the yield for He$^+$ and can restore the more common trend of increased He$^+$ yield versus Ne$^+$. In future work, it might be interesting to supplement our model with rate calculations similar to those performed by Goebl et al. [47] for other elements, so we can weigh the contribution of each orbital accordingly.
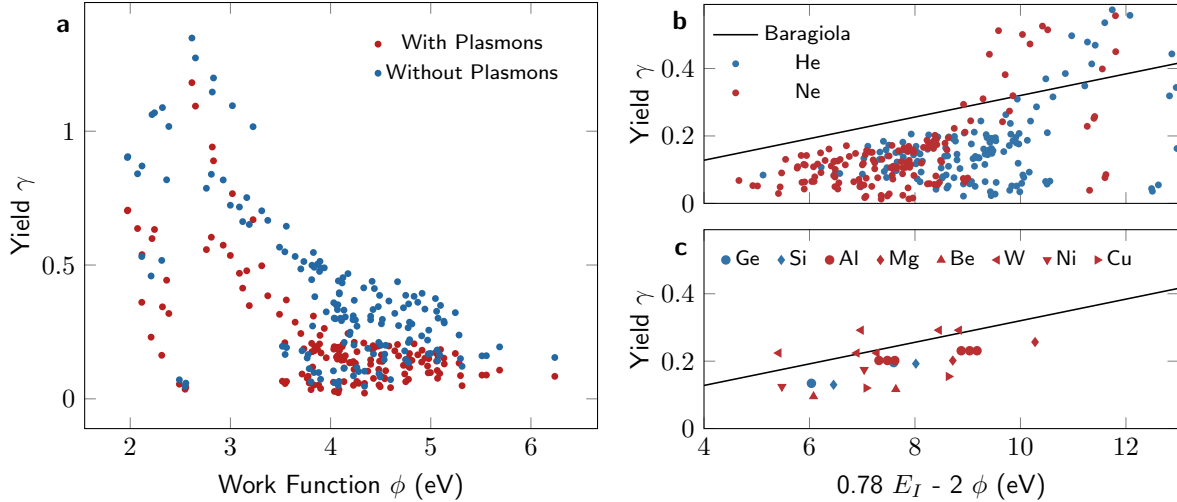


Figure 11: (**a**) Calculated yields of He$^+$ ions incident on all surfaces versus their work function. The regular data, including our model for the plasmonic excitations, is shown in red. For comparison, we have also added the results without plasmonic effects $(\kappa_v = \kappa_s = 0)$ in blue. (**b**) Calculated secondary electron yields compared to the fit of Baragiola et al. [18]. (**c**) Comparison of all experimental yield values available - tabulated in Table 1 - with the fit of Baragiola et al. For materials where we do not know the surface of the corresponding yield result, we have plotted one data point for each experimental work function value.

Figure 11a plots the calculated yield for He$^+$ ions incident on each surface versus its work function, for both the model with and without plasmons. It is clear that the plasmons have a significant influence on the yield for most materials. The work function also has an important influence on the yield, which is to be expected, however we also find that for a single value of the work function there can be a wide range of yields. The fact that this is true for both the results with and without plasmons indicates that this is not simply a consequence of the electronic response of the material, but most likely due to differences in the density of states of the various surfaces.

Finally, in Fig. 11b-c we compare both our calculated yield spectra and work functions, as well as the experimental results tabulated in Table 1, with an empirical fit from Baragiola et

al. [18]:

$$\gamma = 0.032 \left( 0.78 E_I - 2\phi \right). \tag{24}$$

It is clear that for surfaces with higher work functions (left side of the figure), our calculated yields lie consistently below Baragiola's fit. This is also the case for most experimental data, however, with the sole exception of tungsten, for which we observed a significant discrepancy between our calculated spectra and the experimental ones in Sec. 5. For surfaces with lower work functions (right side of Figs. 11b-c), the calculated yield can be significantly higher than the value corresponding to Baragiola's fit. This is another indication that we overestimate the yield of these surfaces due to the excessive efficiency of the electron cascades in our model. As mentioned in section 2, our model solely focuses on the AN process, disregarding the RN/AD route, which has the potential for higher yields. In cases where RN/AD is feasible for specific ion/surface combinations, this approach might lead to underestimating the total yield. However, quantifying the extent of underestimation is challenging.

Besides the results of Hagstrum, Baragiola et al. relied on the results of Oechsner [48] and Arifov [49]. The former, however, used $Ar^+$ ions with a kinetic energy of 1 keV, which can significantly increase the electron yield compared to relatively slow ions (4-100 eV). Since our model does not consider kinetic mechanisms in the calculation of the yield, this could be an explanation as to why our results lie below Baragiola's fit. Finally, considering the importance of plasmon excitations, and the highly material dependent energy loss spectra in Fig. 5, it seems unlikely that an accurate electron yield can be obtained from a linear fit relying solely on the ionization energy $E_I$ and work function $\phi$.

# 7   Conclusions and outlook

Starting from our previous work, we have extended our model with an implementation of plasmonic excitations in order to apply it to metallic surfaces. Here, the model makes a distinction between surface and volume plasmons, both of which play an important role in the secondary electron emission process. The calculated spectra match reasonably well with experiment, but there are some discrepancies, e.g. for Cu and W. Moreover, when applying the model to most group I-II elemental surfaces, the calculated yield is very high, and most likely an overestimation. Finally, due to the electronic structure of the surface, it is possible that for some elements the calculated yield is lower for $He^+$ than $Ne^+$, despite the higher ionization energy of $He^+$.

Although the electron cascades are an important process that allows our model to retrieve the low energy electrons missing in Hagstrum's original model, it is possible that our idealistic representation of the process overestimates the number of cascading electrons that contribute to the total yield. For many elements, this overestimation can be balanced by the fact that we use an isotropic distribution for the wave vector of the excited electron. Hagstrum was right to consider the distribution to be more skewed along the normal of the surface, but most likely overemphasized this effect to obtain sufficient electrons at low energy. In our

case, the fully isotropic distribution means that every excited electron has a lower chance to escape than in Hagstrum's case. This is also true for the I-II group elements, but here the idealistic electron cascades implementation combined with the low work function of their surfaces results in a far greater overestimation.

The model in its current state offers a pragmatic and effective approach for calculating yield spectra, but can still benefit from several improvements. First, using an approach similar to Goebl et al. [47] to calculate transition rates for atomic orbitals can be used to weigh the participation of $s$, $p$ and $d$ electrons. Moreover, if it is possible to extend such calculations to the comparison of the Auger- and resonant neutralization process, it can allow us to include the resonant mechanism in our calculation without introducing more parameters.

Second, the escape probability is modelled using a simple step-potential barrier, which ignores the internal crystalline structure of the surface, the electromagnetic response of the metal to the incoming ion and scattering of valence electrons from the vacuum exterior side. The first two approximations can be improved by considering the derivation of MacColl [50] for a more realistic potential barrier:

$$V(x) = \begin{cases} -V_0 + V_1 \sin[a(x - x_0)], & x \leq x_0 \\ -e^2/(4x), & x > x_0 \end{cases} \tag{25}$$

Here, $V_0$, $V_1$ and $a$ could potentially be derived by fitting them to our calculation of the inner potential, which is currently averaged to obtain the work function of the surface. The scattering of valence electrons is a many-body problem and hence more challenging to model, however some authors have introduced an imaginary part to the potential barrier to describe the inelastic aspects [51, 52]. We refer the reader to [53] for a concise discussion on the topic.

Third, both the implementation of the electron cascades and the plasmonic excitations can be improved by including the wave vector of the electron in the calculation. Finally, the ionization energy can be better described by considering a range of energies that depend on the distance of the ion to the surface when it is neutralized. However, this requires an accurate function for both the ionization energy as well as the probability of neutralization versus the distance.

# 8 Acknowledgments

# References

[1] Y. Motoyama and F. Sato. "Calculation of secondary electron emission yield $\gamma$ from MgO surface". *IEEE Trans. Plasma Sci.* 34 (2006), pp. 336–342. DOI: `10.1109/TPS.2006.872443`.

[2] Y. Cho et al. "First-principles study on secondary electron emission of MgO surface". *J. Appl. Phys.* 101 (2007), p. 083710. DOI: `10.1063/1.2721857`.

[3] D. Depla et al. "Discharge voltage measurements during magnetron sputtering". *Surf. Coatings Technol.* 200 (2006), pp. 4329–4338. DOI: `10.1016/j.surfcoat.2005.02.166`.

[4] D. Depla, S. Mahieu, and R. De Gryse. "Magnetron sputter deposition: Linking discharge voltage with target properties". *Thin Solid Films* 517 (2009), pp. 2825–2839. DOI: `10.1016/j.tsf.2008.11.108`.

[5] L. Vignitchouk et al. "Survival and in-vessel redistribution of beryllium droplets after ITER disruptions". *Nuclear Fusion* 58 (May 2018), p. 076008. DOI: `10.1088/1741-4326/aabeec`.

[6] M Daksha et al. "Material dependent modeling of secondary electron emission coefficients and its effects on PIC/MCC simulation results of capacitive RF plasmas". *Plasma Sources Sci. Technol.* 28 (2019), p. 034002. DOI: `10.1088/1361-6595/ab094f`.

[7] P. S. Kothnur, X. Yuan, and L. L. Raja. "Structure of direct-current microdischarge plasmas in helium". *Appl. Phys. Lett.* 82 (2003), pp. 529–531. DOI: `10.1063/1.1540246`.

[8] P. S. Kothnur and L. L. Raja. "Two-dimensional simulation of a direct-current microhollow cathode discharge". *J. Appl. Phys.* 97 (2005). DOI: `10.1063/1.1849816`.

[9] H. D. Hagstrum. "Electron ejection from Mo by $He^+$, $He^{++}$, and $He_2^+$". *Phys. Rev.* 89 (1953), pp. 244–255. DOI: `10.1103/PhysRev.89.244`.

[10] H. D. Hagstrum. "Theory of auger ejection of electrons from metals by ions". *Phys. Rev.* 96 (1954), pp. 336–365. DOI: `10.1103/PhysRev.96.336`.

[11] H. D. Hagstrum. "Auger electron ejection from germanium and silicon by noble gas ions". *Phys. Rev.* 119 (1960), pp. 940–952. DOI: `10.1103/PhysRev.119.940`.

[12] M. Bercx, B. Partoens, and D. Lamoen. "Quantitative modeling of secondary electron emission from slow-ion bombardment on semiconductors". *Phys. Rev. B* 99 (2019). DOI: `10.1103/physrevb.99.085413`.

[13] C. R. Monreal. "Auger neutralization and ionization processes for charge exchange between slow noble gas atoms and solid surfaces". *Prog. Surf. Sci.* 89 (2014), pp. 80–125. DOI: `10.1016/j.progsurf.2014.01.001`.

[14] R. A. Baragiola and C. A. Dukes. "Plasmon-Assisted Electron Emission from Al and Mg Surfaces by Slow Ions". *Phys. Rev. Lett.* 76 (1996), pp. 2547–2550. DOI: `10.1103/PhysRevLett.76.2547`.

[15] R. A. Baragiola, C. A. Dukes, and P. Riccardi. "Plasmon excitation in ion-solid interactions". In: *Nucl. Instruments Methods Phys. Res. Sect. B Beam Interact. with Mater. Atoms*. Vol. 182. 1-4. North-Holland, 2001, pp. 73–83. DOI: `10.1016/S0168-583X(01)00723-6`.

[16] R. A. Baragiola and R. C. Monreal. "Electron emission from surfaces mediated by ion-induced plasmon excitation". In: *Slow Heavy-Particle Induced Electron Emission from Solid Surfaces*. Vol. 225. Springer Tracts in Modern Physics. Berlin, Heidelberg: Springer Berlin Heidelberg, 2007, pp. 185–211. DOI: `10.1007/3-540-70789-1_6`.

[17] J. Burgdörfer and C. Lemell. "Theoretical concepts and methods for electron emission from solid surfaces". In: *Slow Heavy-Particle Induced Electron Emission from Solid Surfaces*. Vol. 225. Springer Tracts in Modern Physics. Berlin, Heidelberg: Springer, Berlin, Heidelberg, 2007, pp. 1–38. ISBN: 978-3-540-70788-2. DOI: `10.1007/3-540-70789-1_1`.

[18] R. Baragiola et al. "Ion-induced electron emission from clean metals". *Surf. Sci.* 90 (1979), pp. 240–255. DOI: `10.1016/0039-6028(79)90341-8`.

[19] E. V. Alonso et al. "Z1 dependence of ion-induced electron emission from aluminum". *Physical Review B* 22 (July 1980), pp. 80–87. DOI: `10.1103/physrevb.22.80`.

[20] M. A. Cazalilla et al. "Theory of Auger neutralization and deexcitation of slow ions at metal surfaces". *Physical Review B* 58 (Nov. 1998), pp. 13991–14006. DOI: `10.1103/physrevb.58.13991`.

[21] H. D. Hagstrum. "Auger Ejection of Electrons from Tungsten by Noble Gas Ions". *Phys. Rev.* 104 (1956), pp. 317–318. DOI: `10.1103/physrev.104.317`.

[22] H. D. Hagstrum. "Auger Ejection of Electrons from Molybdenum by Noble Gas Ions". *Physical Review* 104 (Nov. 1956), pp. 672–683. DOI: `10.1103/physrev.104.672`.

[23] A. A. Almulhem and M. D. Girardeau. "Theory of ion neutralization at metal surfaces by surface plasmon excitation". *Surf. Sci.* 210 (1989), pp. 138–162. DOI: `10.1016/0039-6028(89)90108-8`.

[24] P. Apell. "Surface plasmon de-excitation of multiply charged ions". *J. Phys. B At. Mol. Opt. Phys.* 21 (1988), pp. 2665–2673. DOI: `10.1088/0953-4075/21/14/019`.

[25] R. Monreal and N. Lorente. "Dynamical screening in Auger processes near metal surfaces". *Phys. Rev. B* 52 (1995), pp. 4760–4763. DOI: `10.1103/PhysRevB.52.4760`.

[26] M. Vicente Alvarez, V. Ponce, and E. Goldberg. "Auger, resonant, and plasmon-assisted charge-transfer processes in atom-surface collisions". *Phys. Rev. B* 57 (1998), pp. 14919–14929. DOI: `10.1103/PhysRevB.57.14919`.

[27] J. Asselin, E. R. Hopper, and E. Ringe. "Improving the stability of plasmonic magnesium nanoparticles in aqueous media". *Nanoscale* 13 (48 2021), pp. 20649–20656. DOI: `10.1039/D1NR06139A`.

[28] N. W. Ashcroft and N. D. Mermin. "Solid State Physics" (1976).

[29] R. H. Ritchie. "Plasma Losses by Fast Electrons in Thin Films". *Phys. Rev.* 106 (1957), pp. 874–881. DOI: `10.1103/PhysRev.106.874`.

[30]  R. F. Egerton. "Electron energy-loss spectroscopy in the TEM". *Reports Prog. Phys.* 72 (2009), p. 016502. DOI: `10.1088/0034-4885/72/1/016502`.

[31]  R. Gallager. *Poisson Processes*. MIT open courseware. 2011.

[32]  H. Raether. *Excitation of Plasmons and Interband Transitions by Electrons.* Springer-Verlag, 1980. DOI: `10.1007/bfb0045951`.

[33]  S. A. Maier. *Plasmonics: Fundamentals and Applications.* Springer US, 2007. DOI: `10.1007/0-387-37825-1`.

[34]  Y. Takeishi and H. D. Hagstrum. "Auger-type electron ejection from the (111) face of nickel by slow He+, Ne+, and Ar+ ions". *Phys. Rev.* 137 (1965). DOI: `10.1103/PhysRev.137.A641`.

[35]  H. D. Hagstrum. "Ion-neutralization spectroscopy of solids and solid surfaces". *Phys. Rev.* 150 (1966), pp. 495–515. DOI: `10.1103/PhysRev.150.495`.

[36]  G. Kresse and J. Hafner. "Ab initio molecular dynamics for liquid metals". *Phys. Rev. B* 47 (1993), pp. 558–561. DOI: `10.1103/PhysRevB.47.558`.

[37]  G. Kresse and J. Furthmüller. "Efficiency of ab-initio total energy calculations for metals and semiconductors using a plane-wave basis set". *Comput. Mater. Sci.* 6 (1996), pp. 15–50. DOI: `10.1016/0927-0256(96)00008-0`.

[38]  G. Kresse and J. Furthmüller. "Efficient iterative schemes for ab initio total-energy calculations using a plane-wave basis set". *Phys. Rev. B - Condens. Matter Mater. Phys.* 54 (1996), pp. 11169–11186. DOI: `10.1103/PhysRevB.54.11169`.

[39]  P. E. Blöchl. "Projector augmented-wave method". *Phys. Rev. B* 50 (1994), pp. 17953–17979. DOI: `10.1103/PhysRevB.50.17953`.

[40]  D. Joubert. "From ultrasoft pseudopotentials to the projector augmented-wave method". *Phys. Rev. B - Condens. Matter Mater. Phys.* 59 (1999), pp. 1758–1775. DOI: `10.1103/PhysRevB.59.1758`.

[41]  J. P. Perdew, K. Burke, and M. Ernzerhof. "Generalized gradient approximation made simple". *Phys. Rev. Lett.* 77 (1996), pp. 3865–3868. DOI: `10.1103/PhysRevLett.77.3865`.

[42]  H. J. Monkhorst and J. D. Pack. "Special points for Brillouin-zone integrations". *Phys. Rev. B* 13 (1976), pp. 5188–5192. DOI: `10.1103/PhysRevB.13.5188`.

[43]  S. De Waele et al. "Error estimates for density-functional theory predictions of surface energy and work function". *Phys. Rev. B* 94 (2016), p. 235418. DOI: `10.1103/PhysRevB.94.235418`.

[44]  P. Tolias. "Analytical expressions for thermophysical properties of solid and liquid beryllium relevant for fusion applications". *Nuclear Materials and Energy* 31 (2022), p. 101195. DOI: `10.1016/j.nme.2022.101195`.

[45]  H. B. Michaelson. "The work function of the elements and its periodicity". *J. Appl. Phys.* 48 (1977), pp. 4729–4733. DOI: `10.1063/1.323539`.

[46]  A. K. Green and E. Bauer. "Work function and purity of the Beryllium (0001) surface". *Surf. Sci.* 74 (1978), pp. 676–681. DOI: `10.1016/0039-6028(78)90023-7`.

[47] D. Goebl et al. "Band structure effects in Auger neutralization of He ions at metal surfaces". *Phys. Rev. B* 84 (2011), p. 165428. DOI: 10.1103/PhysRevB.84.165428.

[48] H. Oechsner. "Electron yields from clean polycrystalline metal surfaces by noble-gas-ion bombardment at energies around 1 keV". *Phys. Rev. B* 17 (1978), pp. 1052–1056. DOI: 10.1103/physrevb.17.1052.

[49] U. A. Arifov. *Interaction of Atomic Particles with a Solid Surface.* Springer US, 1969. DOI: 10.1007/978-1-4899-4809-0.

[50] L. A. MacColl. "On the Reflection of Electrons by Metallic Crystals". *Bell System Technical Journal* 30 (Oct. 1951), pp. 888–906. DOI: 10.1002/j.1538-7305.1951.tb03687.x.

[51] P. M. Echenique et al. "Semiclassical image potential at a solid surface". *Physical Review B* 23 (June 1981), pp. 6486–6493. DOI: 10.1103/physrevb.23.6486.

[52] J Rundgren and G Malmstrom. "Transmission and reflection of low-energy electrons at the surface barrier of a metal". *Journal of Physics C: Solid State Physics* 10 (Dec. 1977), pp. 4671–4687. DOI: 10.1088/0022-3719/10/23/004.

[53] P. Tolias. *Low energy electron reflection from tungsten surfaces.* 2016. DOI: 10.48550/ARXIV.1601.02047.